ARTICLE IN PRESS

INTERNATIONAL JOURNAL OF HYDROGEN ENERGY XXX (XXXX) XXX

Available online at www.sciencedirect.com

ScienceDirect

journal homepage: www.elsevier.com/locate/he

Short Communication

Boosting visible light driven hydrogen production: Bifunctional interface of $Ni(OH)_2$/Pt cocatalyst on TiO_2

Xiaochen Ren [a,c,1], *Fuchun Xu* [a,1], *Zhenbo Peng* [b], *Qianqian Chi* [a], *Wenhao Li* [a], *Jun Wang* [a], *Ting Tao* [a], *Wei Ye* [a,**], *Peng Gao* [a,*]

[a] *College of Material, Chemistry and Chemical Engineering, Hangzhou Normal University, Hangzhou, Zhejiang, 311121, PR China*

[b] *Chemical Engineering College, Ningbo Polytechnic, Ningbo, 315800, PR China*

[c] *School of Materials Science and Engineering, Harbin Engineering University, Harbin, 150001, PR China*

HIGHLIGHTS

- Bifunctional $Ni(OH)_2$/Pt interface was successfully constructed on TiO_2 nanotubes.
- $Ni(OH)_2$/Pt interface facilitates the adsorption of H_2O.
- $Ni(OH)_2$/Pt interface promotes the separation of electron/hole pairs.
- A high visible-light driven hydrogen evolution activity of 5875 $\mu mol\ g^{-1}\ h^{-1}$ was achieved for $Ni(OH)_2/Pt/TiO_2$ sample.

GRAPHICAL ABSTRACT

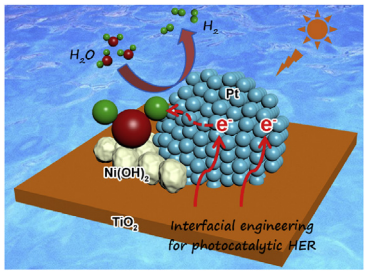

ARTICLE INFO

Article history:
Received 4 November 2019
Received in revised form
12 March 2020
Accepted 11 April 2020
Available online xxx

Keywords:
Interfacial engineering
Bifunctional

ABSTRACT

Sunlight driven hydrogen production by water splitting represents a sustainable approach for hydrogen energy utilization, however, solo semiconductor could not meet the current demand. Herein, as proof of concept, we put forward a bifunctional interface of $Ni(OH)_2$/Pt cocatalyst loaded on anatase TiO_2 through a selective deposition process. $Ni(OH)_2$/Pt interface facilitates H_2O adsorption by providing two adsorption sites: O is selectively adsorbed on $Ni(OH)_2$ and H adsorbed on metallic Pt. Beyond that, $Ni(OH)_2$/Pt interface also extends light absorption range of TiO_2 to visible light region and accelerates the separation of photo-generated electrons/holes for semiconductor TiO_2. Benefiting from this interfacial engineering in semiconductor, the visible-light driven hydrogen production performance

* *Corresponding author.*
** *Corresponding author.*
E-mail addresses: yewei@hznu.edu.cn (W. Ye), gaopeng@hrbeu.edu.cn (P. Gao).

[1] These authors contributed equally.

https://doi.org/10.1016/j.ijhydene.2020.04.090

Please cite this article as: Ren X et al., Boosting visible light driven hydrogen production: Bifunctional interface of $Ni(OH)_2$/Pt cocatalyst on TiO_2, International Journal of Hydrogen Energy, https://doi.org/10.1016/j.ijhydene.2020.04.090

Visible-light driven
Hydrogen production
$Ni(OH)_2$

of the as-obtained $Ni(OH)_2/Pt/TiO_2$ sample is greatly boosted with a rate of 5875 μmol g^{-1} h^{-1}, 2.6 times higher than that of Pt/TiO_2.

Introduction

Solar energy utilization represents a sustainable approach that has a bright future to solve the current energy crisis [1–5]. Hydrogen production from water splitting under sunlight with semiconductor catalysts seems to be the most possible means of implementation [6,7]. Typically, semiconductors usually absorb suitable light to produce electrons/holes, and the active electrons are migrated to the surface of semiconductors to participate reduction reaction (*i.e.*, hydrogen production) [8–10]. However, photocatalytic hydrogen production still suffers from several bottlenecks: *i*) Weak visible-light absorption ability which is determined by the wide band gap of semiconductors. Such as anatase TiO_2, its band gap is up to 3.2 eV and usually only absorbs UV-light, which only accounts for 5% of total energy in the sunlight [11,12]; *ii*) Less photo-generated reactive electrons, which often recombine with holes before migrating to the catalyst surface and participating reactions [13]; *iii*) Insufficient catalytic sites to adsorb and convert water molecule into hydrogen [14,15].

The above bottlenecks for sunlight driven hydrogen production can be greatly alleviated by hybridization of semiconductors with noble metal nanocrystals as cocatalysts. A Schottky junction is naturally formed in metal/semiconductor interface, which facilitates the separation of electrons/holes and provides active sites for hydrogen evolution [16,17]. Pt is seemed as the most active single metallic cocatalyst for hydrogen evolution in acidic medium. H^+ has very low adsorption energy on Pt surface and $2H_{ad}$ are combined to hydrogen via a Tafel step with fast kinetics [18,19]. However, in neutral and alkaline media, water splitting is triggered by adsorption of H_2O and subsequent formation of a reactive hydrogen intermediate H_{ad} in a process of Volmer step ($H_2O + Pt + e^- \rightarrow Pt\text{-}H_{ad} + OH^-$). $2H_{ad}$ are coupled to complete hydrogen evolution reaction followed by Heyrovsky step ($H_2O + e^- + Pt\text{-}H_{ad} \rightarrow H_2 + OH^- + Pt$) or Tafel step ($2Pt\text{-}H_{ad} \rightarrow H_2 + 2\ Pt$) [20]. Stemmed from the above steps with slow kinetics, hydrogen evolution activity is greatly declined in neutral and alkaline media. Therefore, photocatalytic water splitting in neutral and alkaline media always displays much lower activity with solo Pt cocatalysts at the mercy of adsorbed water [21,22]. Recent discoveries in electrochemical water splitting reaction indicate that the existence of $Ni(OH)_2/Pt$ interface can boost hydrogen evolution activity in alkaline media by providing two kinds of adsorption sites for O and H atoms, respectively [23,24]. $Ni(OH)_2$ as the O adsorption site promotes the splitting of HO–H and the $2H_{ad}$ adsorbed on Pt surface are coupled via Tafel path [25]. Therefore, hydrogen evolution ability is boosted as Tafel process possesses fast reaction kinetics.

Enlightened by the above discoveries, $Ni(OH)_2/Pt$ interface seems to be an ideal direction toward efficient hydrogen production in neutral solution. Herein, as a proof of concept, we construct a bifunctional interface of $Ni(OH)_2/Pt$ cocatalyst by coating discrete amorphous $Ni(OH)_2$ layer on Pt loaded TiO_2 nanotube. Different from the conventional Pt cluster decorated $Ni(OH)_2$ nanoparticle cocatalyst ($Pt/Ni(OH)_2/TiO_2$ sample) [26], our catalyst design possess the following unique structure merits: *i*) the direct contact of TiO_2 and Pt (Pt/TiO_2 interface) naturally forms the Schottky junction which can extend light absorption range for TiO_2 to visible light region and have more ability to intensify the separation of photo-generated electron/holes than $Ni(OH)_2/TiO_2$ interface. *ii*) The electron accumulation on Pt site shortens the electron transfer path than $Pt/Ni(OH)_2/TiO_2$ sample as the photo-generated electrons are transformed to $Ni(OH)_2$ and then to Pt. *iii*) $Ni(OH)_2/Pt$ interface provide two kinds of adsorption sites to bind O on $Ni(OH)_2$ and H on Pt sites, respectively. Benefitting from the above merits, the visible-light driven hydrogen production performance for $Ni(OH)_2/Pt/TiO_2$ sample is greatly enhanced in reference with that of Pt/TiO_2, $Ni(OH)_2/TiO_2$ and pristine TiO_2 nanotubes. This work provides a promising approach to construct bifunctional cocatalyst by the combination of interface engineering and Schottky junction.

Experimental

Synthesis of $Ni(OH)_2/Pt/TiO_2$ hybrid nanotubes

High-quality of pristine TiO_2 nanotubes were synthesized according to the previous literature [27]. In order to deposit Pt nanoparticles on TiO_2 nanotubes, the as-obtained TiO_2 (0.5 g) nanotubes were dispersed in H_2PtCl_6 (2.5 mM) aqueous solution, then excess $NaBH_4$ (10.25 mL, 50 mM) aqueous solution were added into the mixture under continuous stir, which ensure the complete reduction of $PtCl_6^{2-}$. The product was separated through centrifugation, washed with water and ethanol three times, respectively. To further cover ultrathin amorphous $Ni(OH)_2$ shell on Pt/TiO_2 nanotubes, 0.5 g Pt/TiO_2 were further dispersed in 50 mL NaOH (0.5 M) and stirred for 2 h, 27 mL $Ni(NO_3)_2$ (10 mM) aqueous solution was added into the mixture drop by drop. After 2 h reaction, the final sample was collected by centrifugation and wished with pure water three times, and dried in vacuum oven at 60 °C. The synthetic protocol for $Ni(OH)_2/TiO_2$ nanotubes was similar with that of $Ni(OH)_2/Pt/TiO_2$ except with 0.5 g TiO_2 nanotubes.

Photocatalytic hydrogen evolution

The photocatalytic hydrogen evolution reaction from water was performed using a commercial online photocatalytic

Please cite this article as: Ren X et al., Boosting visible light driven hydrogen production: Bifunctional interface of $Ni(OH)_2/Pt$ cocatalyst on TiO_2, International Journal of Hydrogen Energy, https://doi.org/10.1016/j.ijhydene.2020.04.090

hydrogen production system (AuLight, Beijing, CEL-SPH2N). Specifically, 0.1 g of $Ni(OH)_2/Pt/TiO_2$ nanotubes were added into a 100 mL aqueous solution containing 80 mL water, 20 mL methanol in a quartz reactor. The openings for the whole system were sealed with septums made of silicone rubber at ambient temperature and pressure. Prior to the reaction, the mixture was evacuated into vacuum and pumped by continuous Ar gas flow several times with stirring to remove O_2 and CO_2 dissolved in the solution. A 300 W xenon arc lamp equipped with 400 nm cut optical filter was used as a light source to trigger the photocatalytic reaction. The actual light intensity in the center of quartz reactor was measured by a visible light radiometer (made in the photoelectric instrument factory of Beijing Normal University, China). The focused light intensity on the liquid surface was maintained to 100 mW cm^{-2}. Gas product (H_2) was analyzed using an online gas chromatograph (SP7800, TCD, molecular sieve 0.5 nm, N_2 carrier, Beijing Keruida Limited) and the actual produced H_2 amount was quantified using an internal standard method.

Results and discussion

In order to investigate the impact of $Ni(OH)_2/Pt$ interface on photocatalytic hydrogen evolution activity, high-quality one dimensional anatase TiO_2 nanotubes with curled layered structures were employed as semiconductor substrates, as shown in Fig. S1. Then, Pt nanoparticles were loaded on TiO_2 nanotubes by a careful reduction of H_2PtCl_6 with $NaBH_4$, as shown in Fig. S2. To further implement the deposition of ultrathin discrete $Ni(OH)_2$ shell, Pt/TiO_2 nanotubes were infiltrated in NaOH aqueous solution and then $Ni(NO_3)_2$ solution was dropwise added. This accurate synthetic protocol ensures the formation of ultrathin $Ni(OH)_2$ shell on Pt/TiO_2 nanotubes and partial exposure of Pt nanoparticles for hydrogen evolution reaction. Fig. 1a shows the powder X-ray diffraction (XRD) patterns of $Ni(OH)_2/Pt/TiO_2$ sample in reference with pristine TiO_2, Pt/TiO_2 and $Ni(OH)_2/TiO_2$ nanotubes. All primary diffraction peaks are well matched with standard anatase TiO_2 (JCPDS No. 21–1272) for all samples. Slightly raised peaks located at 39.8° for $Ni(OH)_2/Pt/TiO_2$ and Pt/TiO_2 samples are attributed to (111) plane of face-centered cubic Pt (JCPDS No. 87–0640). There are no additional peaks could be assigned to $Ni(OH)_2$, maybe due to its amorphous nature and/or low content. The field emission scanning electron microscope (SEM) image in Fig. 1b confirms the excellent one-dimensional structure maintained for $Ni(OH)_2/Pt/TiO_2$ sample. Low resolution transmission electron microscopy (TEM) image in Fig. 1c verifies the existence of Pt nanoparticles and one-dimensional tubular structure.

High resolution TEM (HRTEM) image (Fig. 1d) displays the continuous lattice fringes with a distance of 2.0 Å which can be attributed to Pt (200) plane. Also, lattice fringes with a distance of 3.5 Å (Fig. 1e) are ascribed to (101) plane of anatase TiO_2. Different from the smooth outermost surface for Pt/TiO_2 and pristine TiO_2 nanotubes (Figs. S1 and S2), $Ni(OH)_2/Pt/TiO_2$ nanotubes display rough surfaces, indicating that ultrathin $Ni(OH)_2$ layer with about a thickness of 1.0 nm was successfully coated on the outside after a careful examination in locally amplified HRTEM image (Fig. 1f). There is no obvious lattice fringes for the rough region, indicating that the $Ni(OH)_2$ layer is amorphous. To further verify the crystal nature, we taken out Pt/TiO_2 nanotubes from the standard synthetic protocol, the products are identified to be $Ni(OH)_2$ by XRD pattern (Fig. S3), suggesting that the outmost amorphous layer for $Ni(OH)_2/Pt/TiO_2$ is $Ni(OH)_2$. It should be noted that Pt nanoparticles are not completely covered by amorphous $Ni(OH)_2$ layer (Fig. 1d–f), guaranteeing the existence of abundant $Ni(OH)_2/Pt$ interface. The partial exposure of Pt nanoparticles may be due to the high electrons' concentration on Pt, which leads to its electronegativity and the electrostatic repulsion to $Ni(OH)_2$ [28]. To further investigate the $Ni(OH)_2$ content for $Ni(OH)_2/Pt/TiO_2$ hybrid sample, thermogravimetric (TG) analysis was performed, as shown in Fig. S4. The hybrid sample starts to decompose at 220 °C, which can be assigned to the conversion of $Ni(OH)_2$ to NiO, consistent with the reported result for $Ni(OH)_2$ [29]. And 1.8 wt% weight loss between 220 and 350 °C was achieved, suggesting 9.2 wt% of $Ni(OH)_2$ for $Ni(OH)_2/Pt/TiO_2$ sample. $Ni(OH)_2$ content was also determined by inductively coupled plasma atomic emission spectrometry (ICP-AES) which reveals 8.5 wt% of $Ni(OH)_2$, consistent with TG data.

In order to further investigate the species and chemical state of the elements for the sample, X-ray photoelectron spectroscopy (XPS) measurement was employed. The survey spectrum in Fig. 2a confirms the existence of the elements of Ti, O, Ni and Pt for $Ni(OH)_2/Pt/TiO_2$ sample. The high resolution spectrum (Fig. 2b) reveals the peaks located at 856.1 and 873.6 eV are ascribed to $2p_{3/2}$ and $2p_{1/2}$ of Ni^{2+}, respectively [30]. The binding energy for Ni $2p_{3/2}$ located at 856.1 eV is the characteristic peak for $Ni(OH)_2$ with associated intensive satellite peaks at 862.0 eV and 880.0 eV, further confirming the outermost layer of sample is $Ni(OH)_2$, consistent with XRD and TG results [31,32]. Fig. 2c displays two binding energies at 71.0 and 74.3 eV, which are attributed to be $4f_{7/2}$ and $4f_{5/2}$ of typical Pt^0, respectively. Binding energies located at 458.6 and 464.5 eV (Fig. 2d) are ascribed to $2p_{3/2}$ and $2p_{1/2}$ of Ti^{4+}, respectively. The XPS data of Ti^{4+} and Ni^{2+} manifests that the formation of Pt/TiO_2, $Ni(OH)_2/Pt$ and $Ni(OH)_2/TiO_2$ interfaces will not affect the chemical state of pristine TiO_2 and $Ni(OH)_2$. We also tested specific surface areas of all samples using N_2 adsorption-desorption measurements, $Ni(OH)_2/Pt/TiO_2$ nanotubes exhibit a comparative specific surface area of 146.2 m^2 g^{-1} with that of Pt/TiO_2 (145.7 m^2 g^{-1}), $Ni(OH)_2/TiO_2$ (144.0 m^2 g^{-1}) and TiO_2 samples (140.1 m^2 g^{-1}) (Fig. S5 and Table S1). The cladding of ultrathin $Ni(OH)_2$ layer doesn't shield the whole surface of TiO_2 (Fig. 1e and f). The large specific surface area for $Ni(OH)_2/Pt/TiO_2$ sample inherited from ultrathin TiO_2 nanotubes means that more active catalytic sites are provided for hydrogen evolution reaction.

The formation of $Ni(OH)_2/Pt$ interface provides an ideal platform to investigate the impact of interfacial interaction for Pt cocatalyst on photocatalytic hydrogen production. All photocatalytic hydrogen evolution activities are assessed under simulative visible-light irradiation ($\lambda > 400$ nm) using commercialized photocatalytic reaction system with the same catalyst dosage of 0.1 g and methanol as sacrificial agent. In order to make a better comparison, we have also made $Ni(OH)_2/TiO_2$ nanotubes as reference catalyst (Fig. S6, Table S1). Fig. 3a shows the curves of hydrogen evolution amount

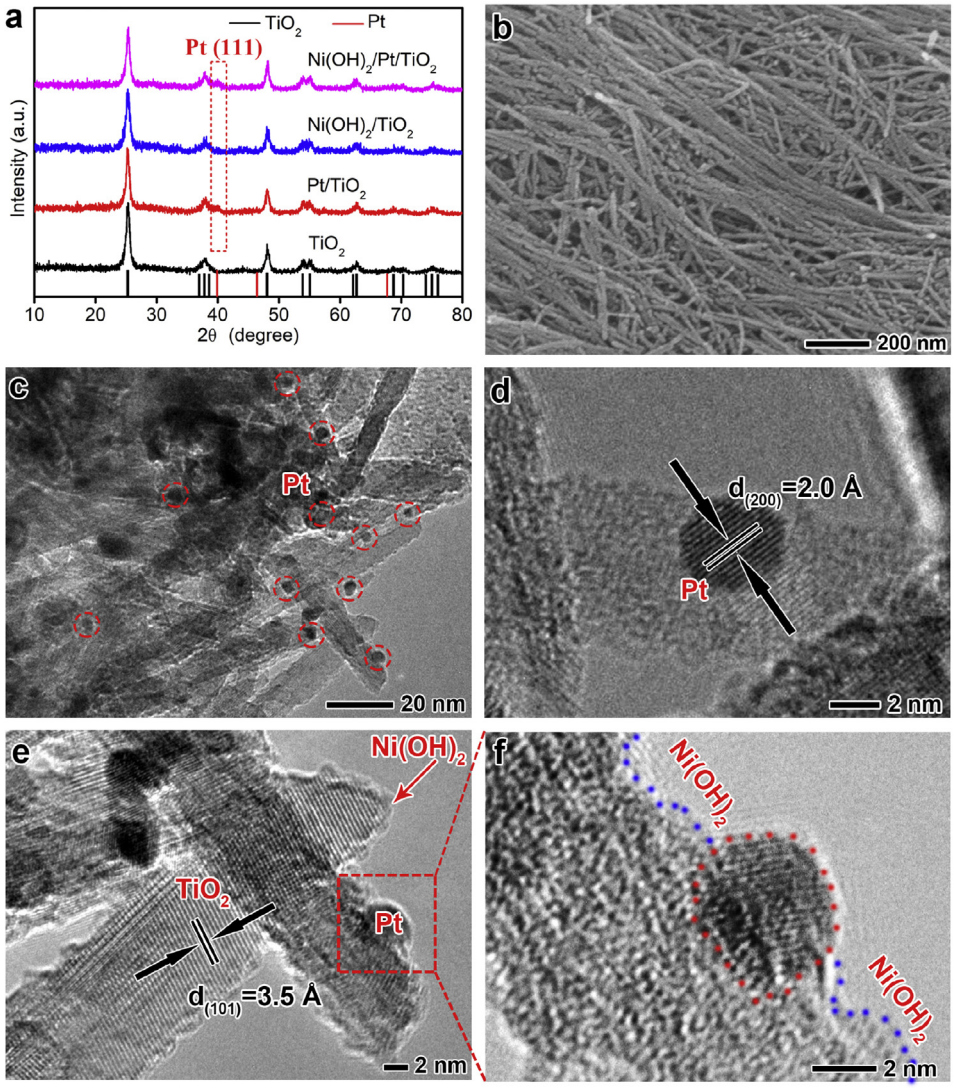

Fig. 1 – (a) Powder X-ray diffraction patterns, (b) scanning electron micrograph, (c) transmission electron photograph, and (d–f) high-solution transmission electron photographs of $Ni(OH)_2/Pt/TiO_2$ hybrid nanotubes.

versus illumination time. For all samples, a linear relationship between hydrogen evolution amount and illumination time indicates that hydrogen is really originated from photocatalytic reaction. Specifically, $Ni(OH)_2/Pt/TiO_2$ sample achieves a hydrogen production rate of 5875 μmol g^{-1} h^{-1}, which is 2.6, 6.4 and 43.8 times higher than that of Pt/TiO_2 (2241 μmol g^{-1} h^{-1}), $Ni(OH)_2/TiO_2$ (912 μmol g^{-1} h^{-1}) and pristine TiO_2 (134 μmol g^{-1} h^{-1}) samples, respectively. The greatly enhanced photocatalytic hydrogen production manifests that the interfacial engineering by the formation of $Ni(OH)_2/Pt$ interface really promotes the hydrogen evolution reaction in neutral solution.

Apart from $Ni(OH)_2/Pt$ interface, the existence of $Ni(OH)_2/TiO_2$ interfacial interaction also contributes to the enhanced hydrogen evolution activity, which is verified by the comparison of different activities of $Ni(OH)_2/TiO_2$ and TiO_2 samples. We also assessed the cycling stability of $Ni(OH)_2/Pt/TiO_2$ catalyst. Our catalyst produces comparable hydrogen amount during the five cycles (25 h), indicating the excellent stability for $Ni(OH)_2/Pt/TiO_2$ nanotubes (Fig. S7).

Upon assessing the photocatalytic hydrogen production activities, it is found that the synergistic effect of $Ni(OH)_2$ and Pt really contributes to the enhanced photocatalytic hydrogen evolution performance. It is well known that Ni^{2+} in $Ni(OH)_2$ interacts with HO–H via Ni^{2+}-$O^{\delta-}$ electrostatic interaction, while H atom binds well with Pt [26,33]. Therefore, $Ni(OH)_2/Pt$ interface strengthens the adsorption of H_2O and promotes its following splitting. And the resulted H_{ad} is recombined to H_2 with the help of Pt catalyst [34]. To verify the synergistic photocatalytic effect in this $Ni(OH)_2/Pt/TiO_2$ system, FT-IR measurement was performed (Figs. 4a and S8). Fig. 4a shows the FT-IR spectra after infinitesimal H_2O adsorption by subtracting the background spectra of samples without H_2O adsorption. The peak located at around 1630 cm^{-1} is the bending vibration mode for adsorbed water molecule [35]. $Ni(OH)_2/Pt/TiO_2$ nanotube possesses a higher bending mode (1638 cm^{-1}) relative to that of Pt/TiO_2 (1627 cm^{-1}) and $Ni(OH)_2/$

Please cite this article as: Ren X et al., Boosting visible light driven hydrogen production: Bifunctional interface of $Ni(OH)_2/Pt$ cocatalyst on TiO_2, International Journal of Hydrogen Energy, https://doi.org/10.1016/j.ijhydene.2020.04.090

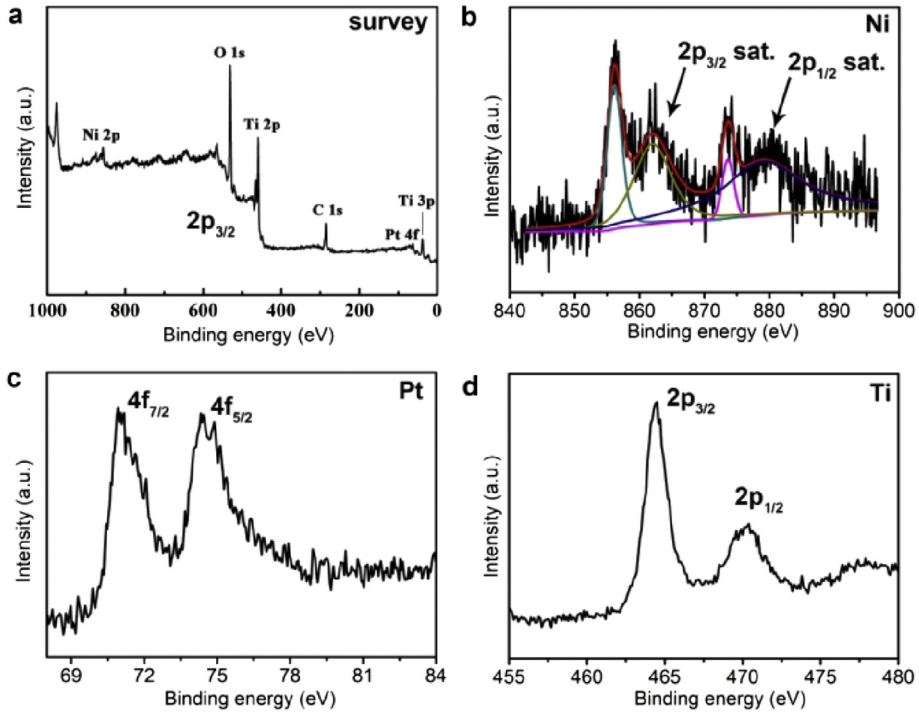

Fig. 2 – X-ray photoelectron spectra of $Ni(OH)_2/Pt/TiO_2$ hybrid nanotubes. (a) Survey, (b) Ni 2p, (c) Pt 4f, (d) Ti 2p.

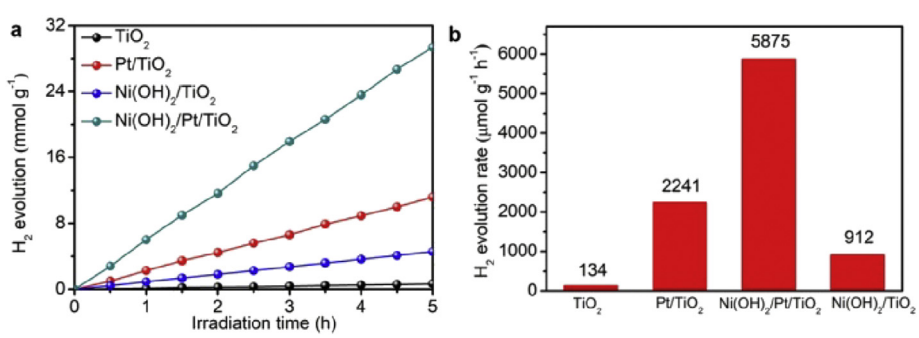

Fig. 3 – (a) The comparison of visible light driven hydrogen production using $Ni(OH)_2/Pt/TiO_2$ hybrid nanotubes as catalysts and methanol as sacrificial agent under the irradiation of visible light (λ > 400 nm) in reference with Pt/TiO_2, $Ni(OH)_2/TiO_2$ and TiO_2 samples.

TiO_2 (1625 cm^{-1}), confirming the synergistic mode of O and H atoms that are fixated on $Ni(OH)_2$/Pt interface, respectively [36]. The promotion effect of the interfacial interaction is also evidenced by Tafel slopes derived from linear sweep voltammetry (LSV) curves recorded in neutral media (Fig. S9). $Ni(OH)_2/Pt/TiO_2$ possesses a Tafel slope of 216 mV dec^{-1}, much lower than that of Pt/TiO_2 sample (299 mV dec^{-1}), suggesting a faster water splitting kinetics [37,38].

Apart from the promotion effect on the enhanced water splitting kinetics, $Ni(OH)_2$/Pt interface also contributes to the visible light absorption. We first assessed the light absorption ability of $Ni(OH)_2/Pt/TiO_2$ catalyst using ultraviolet diffuse reflection spectra in reference with Pt/TiO_2, $Ni(OH)_2/TiO_2$ and pristine TiO_2 samples (Fig. 4c). The deposition of Pt nanoparticles on TiO_2 extends the light absorption range to visible light region, that is because the valence band electrons of TiO_2 are excited to localized energy levels between Pt/TiO_2 interface at wavelength longer than 400 nm [39,40]. $Ni(OH)_2/Pt/TiO_2$ sample exhibits enhanced visible light (400–800 nm) absorption ability compared to Pt/TiO_2 nanotubes. The UV–vis absorption spectra for TiO_2 and $Ni(OH)_2/TiO_2$ samples are almost coincided with each other, indicating that the $Ni(OH)_2/TiO_2$ interface will not greatly impact the visible light absorption ability for TiO_2. Therefore, the enhanced visible light absorption for $Ni(OH)_2/Pt/TiO_2$ sample should be ascribed to the formation of $Ni(OH)_2$/Pt interface. The large electronic affinity of $Ni(OH)_2$ may accelerate the photo-generated electrons to the localized energy level induced by Pt/TiO_2 interface, then visible light absorption ability is enhanced [41].

The band gap for all samples are derived from the transition of Kubelka-Munk function, and $Ni(OH)_2/Pt/TiO_2$ possesses a narrowed band gap of 2.72 eV compared with that of pristine

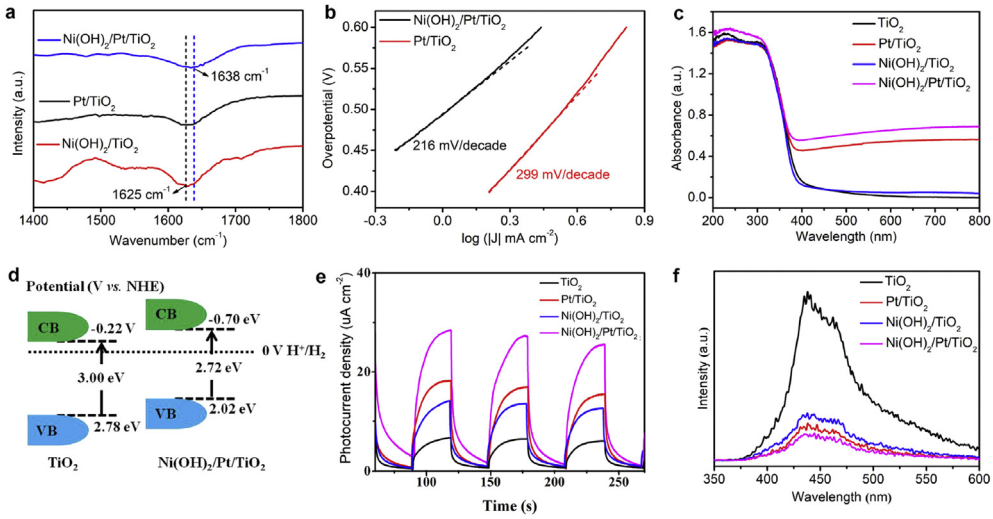

Fig. 4 – (a) Fourier transform infrared spectra of $Ni(OH)_2/Pt/TiO_2$ and Pt/TiO_2 nanotubes after water adsorption. (b) Tafel plots derived from LSV curves recorded in 0.5 M K_2SO_4 solution using $Ni(OH)_2/Pt/TiO_2$ and Pt/TiO_2 nanotubes as catalysts. (c) UV–vis absorption spectra. (d) The electronic band structures of TiO_2 nanotube and $Ni(OH)_2/Pt/TiO_2$ hybrid nanotube. (e) Photocurrent responses versus time (I-t) curves of pristine TiO_2, Pt/TiO_2, $Ni(OH)_2/TiO_2$ and $Ni(OH)_2/Pt/TiO_2$ nanotubes under visible light illumination ($\lambda > 400$ nm) at a bias potential of −0.3 V vs. RHE. (f) Photoluminescence spectra using a 320 nm light as excitation light source.

TiO_2 (3.00 eV). It should be noted that TiO_2 nanotubes display a band gap of 3.00 eV, lower than the intrinsic one (3.20 eV) for TiO_2. That is because our nanotubes possess bits of oxygen defects (Fig. S11), which also explain the visible-light hydrogen evolution ability for TiO_2 nanotubes [42,43]. The narrowed band gap indicates that light absorption cut off is further expended to visible light region. To gain the exact valence band, ultraviolet photoelectron spectroscopy (UPS) measurements are employed and the calculated values are 2.78 and 2.02 eV for TiO_2 and $Ni(OH)_2/Pt/TiO_2$ samples (Fig. S12), respectively. Therefore, the corresponding conduction bands are inferred and shown in Fig. 4d.

The photo-generated electrons are pumped to the surface of Pt nanoparticles due to the relative larger work function of Pt than that of TiO_2, knowing as Schottky junction [44,45]. The separation efficiency of photo-generated electron/holes can be assessed by photocurrent tests. As shown in Fig. 4e, $Ni(OH)_2/Pt/TiO_2$ sample displays a much enhanced photocurrent response than Pt/TiO_2, $Ni(OH)_2/TiO_2$ and TiO_2 samples. The enhanced photocurrent response should be enabled by the following two factors: *i*) The formation of $Ni(OH)_2/Pt$ interface combined with a Schottky junction intensifies the visible-light absorption and induces more photo-generated electrons (Fig. S13). *ii*) The existence of $Ni(OH)_2$ also promotes the separation of carriers for TiO_2 due to its higher electronic transmission ability, as indicated by EIS analysis (Fig. S14) [46,47]. The hypothesis is further verified by comparison the photocurrents of $Ni(OH)_2/TiO_2$ and pristine TiO_2 nanostructures. To further inspect the practical separation efficiency of electrons/holes pairs under visible-light irradiation, steady-state photoluminescence (PL) spectroscopy measurements with a same amount of samples using a 320 nm excitation light have been conducted, as shown in Fig. 4f. $Ni(OH)_2/Pt/TiO_2$ sample possesses the lowest PL intensity in reference with Pt/TiO_2, $Ni(OH)_2/TiO_2$ and TiO_2 samples. The lower emission peak intensity indicates that the recombination of photo-generated electrons/holes is effective suppressed, consistent with the calculated carrier densities, photocurrent and EIS data [48]. To facilitate understanding, the detailed mechanism of the formation of $Ni(OH)_2/Pt$ cocatalyst on TiO_2 nanotubes to boost photocatalytic hydrogen evolution reaction is schematic illustrated in Fig. 5.

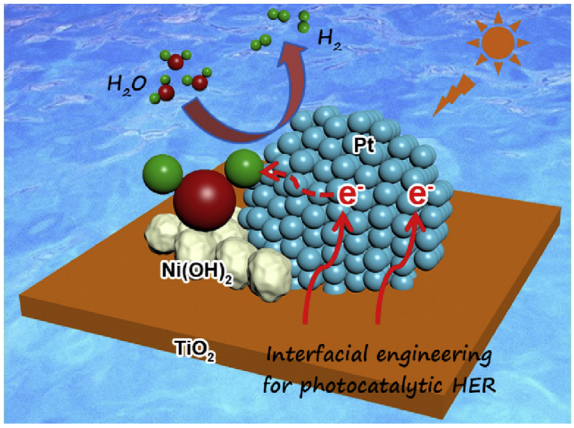

Fig. 5 – Schematic illustration of the mechanism of $Ni(OH)_2/Pt$ cocatalyst on TiO_2 to boost photocatalytic hydrogen evolution reaction.

Conclusions

In summary, we have successfully constructed a $Ni(OH)_2/Pt$ hybrid interface to realize a chemical synergistic mechanism

on promoting water splitting based on their respective interaction to O and H atoms in water. This mechanism is proved by the corresponding FT-IR spectroscopy and electrochemical Tafel measurements. Moreover, $Ni(OH)_2$/Pt interface further enhances the visible light absorption and elevates the separation efficiency of photo-generated electrons/holes. Benefiting from the above merits, $Ni(OH)_2$/Pt/TiO_2 hybrid nanotubes display much improved visible light driven photocatalytic hydrogen evolution performance with a rate of 5875 μmol g^{-1} h^{-1}. This work provides insights into design of highly efficient photocatalyst for visible light driven reaction based on interfacial engineering.

Author contributions

The manuscript was written through contributions of all authors. All authors have given approval to the final version of the manuscript.

Acknowledgment

This work was financially supported in part by the National Natural Science Foundation of China (No. 51902077), Natural Science Foundation of Zhejiang Province (LQ19B010001, LY18E020010), the Funding for scientific research start-up (4095C5021820441, 4095C5021820406) of Hangzhou Normal University, the Pandeng Plan Foundation of Hangzhou Normal University for Youth Scholars of Materials, Chemistry and Chemical Engineering, National College Students' Science and Technology Innovation Project (No. 201910346045, 201910346038, 201910346030), Zhejiang Province "Ten Thousand People Plan", Agricultural and Social Development Program Project (20191203B03) of Hangzhou Science and Technology Bureau of Zhejiang Province, and general items of Zhejiang Provincial Department of Education (Y201840068, Y201533640).

Appendix A. Supplementary data

Supplementary data to this article can be found online at https://doi.org/10.1016/j.ijhydene.2020.04.090.

REFERENCES

[1] Wang Z, Li C, Domen K. Recent developments in heterogeneous photocatalysts for solar-driven overall water splitting. Chem Soc Rev 2019;48:2109–25.
[2] Acar C, Bicer Y, Demir ME, Dincer I. Transition to a new era with light-based hydrogen production for a carbon-free society: an overview. Int J Hydrogen Energy 2019;44:25347–64.
[3] Ahmed M, Dincer I. A review on photoelectrochemical hydrogen production systems: challenges and future directions. Int J Hydrogen Energy 2019;44:2474–507.
[4] Prasad C, Tang H, Liu QQ, Bahadur I, Karlapudi S, Jiang YJ. A latest overview on photocatalytic application of g-C_3N_4 based nanostructured materials for hydrogen production. Int J Hydrogen Energy 2020;45:337–79.
[5] Zhang Y, Ng S, Lu X, Zheng Z. Solution-processed transparent electrodes for emerging thin-film solar cells. Chem Rev 2020;120:2049–122.
[6] Chen X, Shen S, Guo L, Mao SS. Semiconductor-based photocatalytic hydrogen generation. Chem Rev 2010;110:6503–70.
[7] Jayakumar J, Chou H. Recent advances in visible-light-driven hydrogen evolution from water using polymer photocatalysts. ChemCatChem 2019. https://doi.org/10.1002/cctc.201901725.
[8] Bai S, Jiang J, Zhang Q, Xiong Y. Steering charge kinetics in photocatalysis: intersection of materials syntheses, characterization techniques and theoretical simulations. Chem Soc Rev 2015;44:2893–939.
[9] Yu Z, Liu H, Zhu M, Li Y, Li W. Interfacial charge transport in 1D TiO_2 based photoelectrodes for photoelectrochemical water splitting. Small 2019:1903378.
[10] Dong G, Qiu P, Meng F, Wang Y, He B, Yu Y, Liu X, Li Z. Facile synthesis of sulfur-doped polymeric carbon nitride/MoS_2 face-to-face heterojunction for highly efficient photocatalytic interfacial charge separation. Chem Eng J 2020;384:123330.
[11] Daude N, Gout C, Jouanin C. Electronic band structure of titanium dioxide. Phys Rev B 1977;15:3229–35.
[12] Sun S, Chi Q, Zhou H, Ye W, Zhu G, Gao P. A continuous valence band through N-O orbital hybridization in N-TiO_2 and its induced full visible-light absorption for photocatalytic hydrogen production. Int J Hydrogen Energy 2019;44:3553–9.
[13] Xu XS, Guo YC, Liang ZQ, Cui HZ, Tian J. Remarkable charge separation and photocatalytic efficiency enhancement through TiO_2(B)/anatase hetrophase junctions of TiO_2 nanobelts. Int J Hydrogen Energy 2019;44:27311–8.
[14] Tian L, Min S, Wang F, Zhang Z. Metallic vanadium nitride as a noble-metal-free cocatalyst efficiently catalyzes photocatalytic hydrogen production with CdS nanoparticles under visible light irradiation. J Phys Chem C 2019;123:28640–50.
[15] Zhang J, Yu Z, Gao Z, Ge H, Zhao S, Chen C, Chen S, Tong X, Wang M, Zheng Z, Qin Y. Porous TiO_2 nanotubes with spatially separated platinum and CoO_x cocatalysts produced by atomic layer deposition for photocatalytic hydrogen production. Angew Chem Int Ed 2017;56:816–20.
[16] Yang J, Wang D, Han H, Li C. Roles of cocatalysts in photocatalysis and photoelectrocatalysis. Acc Chem Res 2013;46:1900–9.
[17] Yin YC, Xu C, Liu ZB, Ren WC, Sun CH. Ultrathin alpha-Mo_2C dominated by (100) Surface/Cu Schottky junction as efficient catalyst for hydrogen evolution. Int J Hydrogen Energy 2019;44:853–9.
[18] Nørskov JK, bligaard T, Rossmeis J, Christensen CH. Towards the computational design of solid catalysts. Nat Chem 2009;1:37–46.
[19] Greeley J, Nørskov JK. Large-scale, density functional theory-based screening of alloys for hydrogen evolution. Surf Sci 2007;601:1590–8.
[20] Kavian R, Choi S, Park J, Liu T, Peng H, Lu N, Wang J, Kim MJ, Xia Y, Lee SW. Pt-Ni octahedral nanocrystals as a class of highly active electrocatalysts toward the hydrogen evolution reaction in an alkaline electrolyte. J Mater Chem A 2016;4:12392–7.
[21] Durst J, Siebel A, Simon C, Hasché F, Herranz J, Gasteiger HA. New insights into the electrochemical hydrogen oxidation and evolution reaction mechanism. Energy Environ Sci 2014;7:2255–60.

[22] Markovića NM, Sarraf ST, Gasteiger HA, Ross PN. Hydrogen electrochemistry on platinum low-index single-crystal surfaces in alkaline solution. J. Chem. Soc. Faraday Trans 1996;92:3719–25.
[23] Subbaraman R, Tripkovic D, Strmcnik D, Chang K, Uchimura M, Paulikas AP, Stamenkovic V, Markovic NM. Enhancing hydrogen evolution activity in water splitting by tailoring Li^+-$Ni(OH)_2$-Pt interfaces. Science 2011;334:1256–60.
[24] Yin H, Zhao S, Zhao K, Muqsit A, Tang H, Chang L, Zhao H, Gao Y, Tang Z. Ultrathin platinum nanowires grown on single-layered nickel hydroxide with high hydrogen evolution activity. Nat Commun 2015;6:6430.
[25] Ye W, Ren C, Liu D, Wang C, Zhang N, Yan W, Song L, Xiong Y. Maneuvering charge polarization and transport in 2H-MoS_2 for enhanced electrocatalytic hydrogen evolution reaction. Nano Res 2016;9:2662–71.
[26] Sun S, Zhang Y, Shen G, Wang Y, Liu X, Duan Z, Pan L, Zhang X, Zou J. Photoinduced composite of Pt decorated $Ni(OH)_2$ as strongly synergetic cocatalyst to boost H_2O activation for photocatalytic overall water splitting. Appl Catal B: Environ 2019;243:253–61.
[27] Liu W, Gao P, Bao D, Zhang G, Chen Y, Chen G, Wang Y, Wang L, Yang S, Li G, Sun Y. Topotactic conversion route to ultrafine crystalline TiO_2 nanotubes with optimizable electrochemical performance. RSC Adv 2013;3:6531–7.
[28] Chen G, Xu C, Huang X, Ye J, Gu L, Li G, Tang Z, Wu B, Yang H, Zhao Z, Zhou Z, Fu G, Zheng N. Interfacial electronic effects control the reaction selectivity of platinum catalysts. Nat Mater 2016;15:564–9.
[29] Aghazadeh M, Nozad Golikand A, Ghaemi M. Synthesis, characterization, and electrochemical properties of ultrafine β-$Ni(OH)_2$ nanoparticles. Int J Hydrogen Energy 2011;36:8674–9.
[30] Fu Y, Song J, Zhu Y, Cao C. High-performance supercapacitor electrode based on amorphous mesoporous $Ni(OH)_2$ nanoboxes. J Power Sources 2014;262:344–8.
[31] Zhong J, Wang A, Li G, Wang J, Ou Y, Tong Y. Co_3O_4/$Ni(OH)_2$ composite mesoporous nanosheet networks as a promising electrode for supercapacitor applications. J Mater Chem 2012;22:5656–65.
[32] Mansour AN. Characterization of β-$Ni(OH)_2$ by XPS. Surf Sci Spectra 1994;3:239–46.
[33] Nørskov JK, Bligaard T, Logadottir A, Kitchin JR, Chen JG, Pandelov S, Stimming U. Trends in the exchange current for hydrogen evolution. J Electrochem Soc 2005;152:23–6.
[34] Subbaraman R, Tripkovic D, Chang K, Strmcnik D, Paulikas AP, Hirunsit P, Chan M, Greeley J, Stamenkovic V, Markovic NM. Trends in activity for the water electrolyser reactions on 3d M(Ni, Co, Fe, Mn) hydr(oxy)oxide catalysts. Nat Mater 2012;11:550–7.
[35] Iwasita T, Xia X. Adsorption of water at Pt(111) electrode in $HClO_4$ solutions. The potential of zero charge. J Electroanal Chem 1996;411:95–102.
[36] Bordiga S, Regli L, Lamberti C, Zecchina A. FTIR adsorption studies of H_2O and CH_3OH in the isostructural H-SSZ-13 and H-SAPO-34: formation of H-bonded adducts and protonated clusters. J Phys Chem B 2005;109:7724–32.
[37] Li K, Zhang J, Wu R, Yu Y, Zhang B. Anchoring CoO domains on $CoSe_2$ nanobelts as bifunctional electrocatalysts for overall water splitting in neutral media. Adv Sci 2016;3:1500426.
[38] Li Y, Wang H, Xie L, Liang Y, Hong G, Dai H. MoS_2 nanoparticles grown on graphene: an advanced catalyst for the hydrogen evolution reaction. J Am Chem Soc 2011;133:7296–9.
[39] Sakthivel S, Shankar MV, Palanichamy M, Arabindoo B, Bahnemann DW, Murugesan V. Enhancement of photocatalytic activity by metal deposition: characterisation and photonic efficiency of Pt, Au and Pd deposited on TiO_2 catalyst. Water Res 2004;38:3001–8.
[40] Maicu M, Hidalgo MC, Colón G, Navío JA. Comparative study of the photodeposition of Pt, Au and Pd on pre-sulphated TiO_2 for the photocatalytic decomposition of phenol. J. Photochem. Photobiol. A: Chem 2011;217:275–83.
[41] Lee JW, Ahn T, Soundararajan D, Ko JM, Kim J. Non-aqueous approach to the preparation of reduced graphene oxide/α-$Ni(OH)_2$ hybrid composites and their high capacitance behavior. Chem. Commun 2011;47:6305–7.
[42] Yang Y, Gao P, Ren X, Sha L, Yang P, Zhang J, Chen Y, Yang L. Massive Ti^{3+} self-doped by the injected electrons from external Pt and the efficient photocatalytic hydrogen production under visible-Light. Appl Catal B: Environ 2017;218:751–7.
[43] Zhang W, He H, Tian Y, Li H, Lan K, Zu L, Xia Y, Duan L, Li W, Zhao D. Defect-engineering of mesoporous TiO_2 microspheres with phase junctions for efficient visible-light driven fuel production. Nano Energy 2019;66:104113.
[44] Chen H, Chen S, Quan X, Zhang Y. Structuring a TiO_2-based photonic crystal photocatalyst with Schottky junction for efficient photocatalysis. Environ Sci Technol 2010;44:451–5.
[45] Ling YH, Ren FJ, Feng JY. Reverse bias voltage dependent hydrogen sensing properties on Au-TiO_2 nanotubes Schottky barrier diodes. Int J Hydrogen Energy 2016;41:7691–8.
[46] Yu J, Hai Y, Cheng B. Enhanced photocatalytic H_2-production activity of TiO_2 by $Ni(OH)_2$ cluster modification. J Phys Chem C 2011;115:4953–8.
[47] Yuan Y, Xia X, Wu J, Yang J, Chen Y, Guo S. Nickel foam-supported porous $Ni(OH)_2$/NiOOH composite film as advanced pseudocapacitor material. Electrochim Acta 2011;56:2627–32.
[48] Zhang N, Liu S, Fu X, Xu Y. Synthesis of M@TiO_2 (M=Au, Pd, Pt) core-shell nanocomposites with tunable photoreactivity. J Phys Chem C 2011;115:9136–45.

Please cite this article as: Ren X et al., Boosting visible light driven hydrogen production: Bifunctional interface of $Ni(OH)_2$/Pt cocatalyst on TiO_2, International Journal of Hydrogen Energy, https://doi.org/10.1016/j.ijhydene.2020.04.090